


PAPER

[View Article Online](#)
[View Journal](#) | [View Issue](#)Cite this: *Dalton Trans.*, 2022, **51**,
11152Thermodynamics of metallocene catalyst
activation: alignment of theory and experiment†Mikko Linnolahti * and Scott Collins ‡

Three equilibria involved in metallocene catalyst activation, including dissociation of R_2Al_2 ($R = Me, Et$ or $i-Bu$) and related species such as $[L_2ZrMe_2AlMe_2][B(C_6F_5)_4]$ ($L_2 = Cp_2, 1,2$ -ethylenebis(η^5 -indenyl), $Me_2C(\eta^5-C_5H_4)_2$) or $[(L_2ZrMe)_2\mu-Me][MePBB]$ ($L_2 = (h^5-1,2-Me_2C_5H_3)_2$, $[MePBB]^- = [MeB(Ar_F)_3]^-$ with $Ar_F = o-C_6F_5-C_6F_4$) are studied by DFT using various approaches to account for the enthalpy and entropy changes in gas and condensed phases. These studies reveal that both low energy vibrations and translational entropy conspire to cause significant deviations between theory and experiment when it comes to the free energy change in condensed or even gas phase. Alignment of theory with experiment requires in addition, consideration of specific solvation of reactants and products.

Received 1st June 2022,

Accepted 4th July 2022

DOI: 10.1039/d2dt01711c

rsc.li/dalton

Introduction

Over the past several years there has been renewed study of the structure and reactivity of large aluminoxane structures with formulae $(MeAlO)_n(Me_3Al)_m$.¹ These are thought to be models for methylaluminoxane (MAO), and in particular for the active components of that mixture, as MAO is commonly used to activate group 4 metallocene and other single site catalysts for olefin polymerization.²

Previous computational studies have focused on systematic evaluation of the structure of MAO,³ including following its formation *via* hydrolysis of Me_3Al .⁴ The growth of MAO oligomers has been demonstrated to start out as linear aggregates, rings and sheet structures with tetrahedral Al and trigonal O.⁵ Hydrolysis studies of the initial steps have employed MP2 level of theory, while in subsequent work, approaching the experimentally relevant size-domain,⁶ we adopted the more cost-effective M06-2X DFT method,⁷ combined with a basis set of triple zeta quality,⁸ since this functional is well known to treat dispersion forces in the $Al-\mu-Me-Al$ or $(\mu^4-O)Al_4$ bonding found in the structures.⁹

Transition from sheets to cages was initially proposed at *ca.* $n \sim 13$, and a stable cage was located with $n = 16$ and $m = 6$,⁶ which corresponds to the composition of the most intense anion detected by ESI MS upon reaction of hydrolytic MAO with Lewis bases, including metallocene complexes.¹⁰

However, some of the Me_3Al was incorporated as structural $Me_3Al^{1d,e,11}$ – *i.e.* as linear but aggregated $Me_2Al(OAlMe)_xMe$ moieties in this unstrained cage rather than terminal OAl_2Me_5 groups. Based on the number of readily exchangeable Al-Me groups as detected using *e.g.* Et_3Al and ESI-MS,¹² the cage structure did not seem reasonable. This guided us toward a more detailed investigation of the structural motifs, revealing that transition from sheets to cages does not take place at $n \leq 18$. The reason for the preference of sheets over isomeric cages lies in significantly higher entropy, and hence lower free energy, of the sheets. An especially stable sheet anion $[(MeAlO)_{16}(Me_3Al)_6Me]^-$ (hereinafter **[16,6]**[−]) along with its neutral **16,6** precursor does possess the requisite number of exchangeable Al-Me groups.¹³

Accurate calculation of entropy, and thus free energy, requires special attention. As systems get large, the number of low energy normal modes increase dramatically and to the point where it is difficult to estimate their energy, and thus the vibrational entropy using a harmonic oscillator approximation. This is a general and well-known problem, for which quasi-harmonic entropy corrections have been proposed, *e.g.* by raising the problematic low energy vibrations to a cut-off frequency of 100 cm^{-1} .¹⁴

We noticed the importance of this particularly for isomeric structures differing little in the arrangement of the constituent atoms (*i.e.*, conformers) as in recently proposed contact ion-pairs (CIP) between Cp_2ZrMe_2 and our new sheet model for **16,6** (Fig. 1).¹⁵

The calculated TS values of these isomers had a variation of $\sigma = \pm 6.1\text{ kJ mol}^{-1}$ at 298 K. Though the standard deviation is small compared with the total entropy for these large systems (*ca.* 0.75%), in free energy terms this corresponds to a significant amount and might overwhelm attempts to characterize

Department of Chemistry, University of Eastern Finland, Joensuu Campus, Yliopistokatu 7, FI-80100, Joensuu, Finland. E-mail: mikko.linnolahti@uef.fi

† Electronic supplementary information (ESI) available. See DOI: <https://doi.org/10.1039/d2dt01711c>

‡ Former address: Department of Chemistry, University of Victoria, 3800 Finnerty Rd. Victoria, BC.

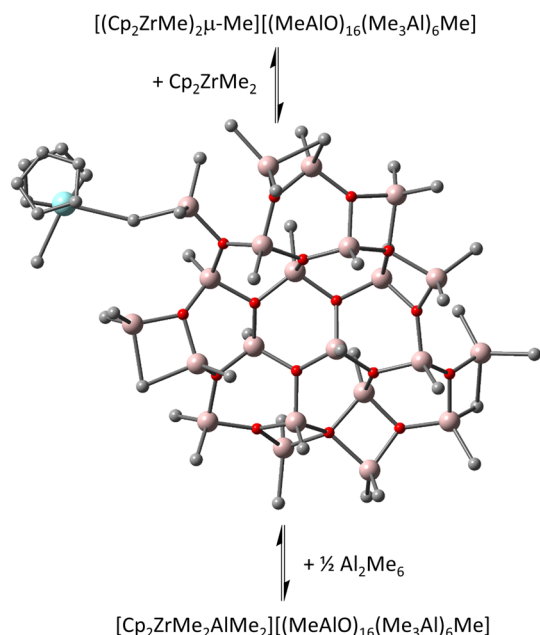


Fig. 1 Equilibria involving contact ion-pair to form outer-sphere ion-pairs detected spectroscopically.¹⁵ Zr in blue, Al in pink, O in red, C in grey, H omitted for clarity.

the reactivity of these large structures in gas phase but also importantly in solution. For example, outer-sphere ion-pairs (OSIP) that have been detected spectroscopically in the case of the Cp_2ZrMe_2 -MAO system include $[\text{Cp}_2\text{ZrMe}_2\text{AlMe}_2][\mathbf{16,6}]$ and $[(\text{Cp}_2\text{ZrMe})_2\mu\text{-Me}][\mathbf{16,6}]$ ¹⁵ and yet the equilibria between these species and any contact ion-pairs present are not as well-documented, in contrast to other ion-pairs featuring well-defined counter-anions.²

Accurate computation of thermodynamic quantities in solution is a topic of great difficulty and debate – we cannot provide here an in-depth discussion but refer the reader to recent literature.¹⁶ We begin by noting that movements become more restricted when moving from gas-phase to solution, thereby reducing the total entropy. Hence, an approximate estimate for the solution Gibbs energy can be obtained by simply scaling the gas-phase entropy, where a $\frac{2}{3}\text{TS}$ scaling factor has been previously employed in the context of metallocenium ion-pair complexes.¹⁷ A more accurate description of specific solvents effects can be obtained by using quantum mechanical continuum solvation models,¹⁸ although these generally do not account for specific solvation of reactants *vs.* products nor effects arising from solvation such as perturbation to the thermodynamically most stable gas phase conformation. Furthermore, the continuum models do not generally account for the restricted movements in solution, and hence the entropies determined in continuum need to be further corrected, particularly for the sake of proper estimation of translational entropy.¹⁹

This prompted us to investigate this issue in more detail and for relevant catalyst activation or other reactions for which thermodynamic data was available, ideally in both gas and

condensed phases. In this paper, we discuss three different reversible reactions involving both neutral species and metallocenium ion-pairs that have been studied experimentally.

Results and discussion

Dissociation of R_6Al_2

The first equilibrium involving dissociation of R_6Al_2 ($\text{R} = \text{Me}$, Et or $i\text{-Bu}$) in gas or condensed phases has been studied in detail.²⁰ For $\text{R} = \text{Me}$, there is general agreement as to the energetics of this process in gas phase with $\Delta H = 84.2$ to 85.4 kJ mol^{-1} , $\Delta S = 177(2) \text{ J mol}^{-1} \text{ K}^{-1}$ and $\Delta G = 31.6(0.3) \text{ kJ mol}^{-1}$ at 298 K (Table 1, entries 1 and 2).²¹ The enthalpy change is accurately estimated at the M06-2X/TZVP level of theory with $\Delta H = 84.9 \text{ kJ mol}^{-1}$. In the case of entropy, consideration of symmetry is required for technical correctness, because of its effect on rotational entropy.^{9,22} However, constraining Me_3Al to C_{3h} -symmetry increases the gas-phase ΔS from 244 to $282 \text{ J mol}^{-1} \text{ K}^{-1}$.

The calculated reaction entropy is thus significantly larger than measured, and even more so in C_{3h} -symmetry. The origin of the increase lies in the low energy normal modes, which gain significant population at $T = 298 \text{ K}$.

While the rotational entropy of Me_3Al decreases, as it should, on constraining to C_{3h} (108.9 to $99.7 \text{ J mol}^{-1} \text{ K}^{-1}$), it is over-compensated by an increase in vibrational entropy (112.6 to $141.0 \text{ J mol}^{-1} \text{ K}^{-1}$) due to minute changes in low energy normal modes, which cannot be calculated to precision using a harmonic oscillator approximation.

We tested Truhlar's quasi-harmonic (qh) entropy correction¹⁴ as a potential remedy for this problem, using a cut-off frequency of 100 cm^{-1} . The correction has a marked effect, reducing the reaction entropy from $\Delta S = 282 \text{ J mol}^{-1} \text{ K}^{-1}$ to $\Delta S\text{-qh} = 188 \text{ J mol}^{-1} \text{ K}^{-1}$, thus bringing it close to the experimental value of $177 \text{ J mol}^{-1} \text{ K}^{-1}$.

The low energy modes also influence the zero-point correction to the electronic energy. Using a similar correction,²³ $\Delta H = 84.9 \text{ kJ mol}^{-1}$ reduces to $\Delta H\text{-qh} = 82.7 \text{ kJ mol}^{-1}$, indicating that the M06-2X/TZVP level of theory underestimates ΔH by $2\text{--}3 \text{ kJ mol}^{-1}$. Thus, our best estimate for the free energy change in gas phase is $\Delta G\text{-qh} = 26.7 \text{ kJ mol}^{-1}$ at 298 K which is within 5 kJ mol^{-1} of the experimental value extrapolated from studies at higher T . For greater certainty we estimated $\Delta G\text{-qh}$ at 418 K in the range covered by experiment, and reasonable agreement is observed (Table 1, entry 6 *vs.* entry 3).

For $\text{R} = \text{Et}$, the dissociation equilibrium has been studied in condensed phase by several techniques (*vide infra*), though some data obtained in gas phase reported in a thesis²⁴ were disseminated in a paper by Smith.²⁵ A plot of $\ln K_d$ *vs.* $1/T$ was non-linear for Et_3Al over the temperature range studied, consistent with decomposition at higher temperatures. Thus, gas phase values of ΔH and ΔS over the T range studied are not available. At the lowest T examined (418 K) $\Delta G = 1.3(2) \text{ kJ mol}^{-1}$ with estimates of $\Delta H = 76(1) \text{ kJ mol}^{-1}$ and $\Delta S = 190(3) \text{ J mol}^{-1} \text{ K}^{-1}$ based on studies of the liquid phase (*vide infra*).



Table 1 Experiment vs. theory for dissociation of R_6Al_2 in gas phase^a

Entry	R	<i>T</i> (K)	ΔH	ΔS	ΔG	ΔH -qh ^b	ΔS -qh ^b	ΔG -qh ^b	Ref.
1	Me	298	85(1)	—	—	—	—	—	21a
2	Me	298	84.2(7)	177(2)	31.6(3)	—	—	—	21b
3	Me	418	84.2(7)	177(2)	10.4(1)	—	—	—	21b
4	Et	418	76(1)	190(3)	1.3(2)	—	—	—	25
5	Me	298	84.9	282.5	0.6	82.7	187.8	26.7	This work
6	Me	418	83.5	278.7	−33.0	80.3	183.8	3.4	This work
7	Et	418	87.8	231.1	−8.8	86.0	203.6	0.8	This work

^a ΔG and ΔH in kJ mol^{-1} , ΔS in $\text{J mol}^{-1} \text{K}^{-1}$ with estimated standard deviation in parentheses for experimental data (entries 1–4). ^b Corrected for low energy vibrations using a quasi-harmonic approach.

We calculated using the quasi-harmonic correction for both H and S that ΔG -qh = 0.8 kJ mol^{-1} , which is in almost precise, though probably fortuitous agreement with the experimental value, as indicated by the larger deviations from experiment for ΔH -qh = 86.0 kJ mol^{-1} and ΔS -qh = $203.6 \text{ J mol}^{-1} \text{K}^{-1}$ at 418 K (Table 1, entries 7 vs. 4).

However, the experimental estimates are not based on the T dependence of K_d so we cannot attach too much significance to these discrepancies, except to state that we did not consider more than one conformer when calculating thermodynamic properties.²⁶

In condensed phase, experimental thermodynamic data for dissociation of liquid R_6Al_2 and solutions in aromatic or aliphatic hydrocarbons differ significantly (Table 2). Beginning with $^i\text{Bu}_3\text{Al}$, it is widely known that this compound is appreciably dissociated in condensed phase, and the accepted values in the liquid phase or hydrocarbon solution are reported in Table 2, entry 1.²⁷

The situation with Et_3Al is complicated by the technique used to determine the dissociation constants, and the temperature range over which the data was collected. The most widely cited values were reported by Smith in papers where calorimetry was used to measure the heat of dilution of this material in both hydrocarbon²⁵ and aromatic hydrocarbon²⁸ solution over a wide temperature range. His data are summarized in entries 2 and 3 where the enthalpy of dissociation is significantly lower in aromatic vs. saturated hydrocarbon media. Later work by Černý and co-workers utilized ^{27}Al NMR

spectroscopy to study this equilibrium.²⁹ Despite collecting data over a similar temperature range (25–100 °C) these workers only analyzed their data between 60–100 °C. Their estimates of ΔG based on this data (entries 4 and 5) differ significantly from those reported by Smith.

Finally, the situation for Me_3Al in condensed phase is the most confusing. Černý and co-workers also studied this equilibrium using ^{27}Al NMR spectroscopy.^{29b} The quality of the data, particularly in mesitylene solution, is not as high as that reported for Et_3Al and moreover these authors concluded that there was little difference in either the enthalpy or entropy of dissociation in comparing aromatic vs. saturated hydrocarbon solution, despite the fact that Et_3Al is more dissociated under the former conditions with a significant difference in ΔG at 298 K according to Smith.

In earlier work, Smith could not use calorimetry to study this equilibrium as Me_3Al is less dissociated than Et_3Al under all conditions.²⁵ He provided estimates based on a number of reasonable assumptions but none of the estimates are based on actual measurement of the equilibrium in question. The available data are summarized in Table 2, entries 6–9.

If we focus on the entropy change for these reactions in hydrocarbon media, those values reported by Smith for $^i\text{Bu}_3\text{Al}$ ($\Delta S = 128(1) \text{ J mol}^{-1} \text{K}^{-1}$), Et_3Al (135(3)) and that estimated for Me_3Al (122(1)) compared with gas phase values of 177(2) and 190(3) for Me_3Al and Et_3Al , or theoretical estimates (*vide infra*) appear reasonable. The much lower values reported by Černý and co-workers (entries 4–5 and 6–7) do not, and suggest an

Table 2 Experimental data for dissociation of R_6Al_2 in condensed phase^a

Entry	R	ΔT (°C)	ΔH	ΔS	ΔG^b	ΔG^c	Solvent	Ref.
1	^iBu	10–45	34.1(5)	128(1)	−3.92(4)	—	^d	27
2	Et	60–150	71(1)	135(3)	—	30.5(6)	^d	25
3	Et	60–150	55.7(5)	100(2)	—	25.9(5)	^e	28
4	Et	60–100	44(5)	69(26)	23(0)	23(9)	^f	29a
5	Et	60–100	40(2)	65(12)	20(7)	20(4)	^g	29a
6	Me	40–100	54(2)	74(6)	32(2)	32(3)	^f	29b
7	Me	40–100	55(6)	81(16)	30(5)	31(6)	^e	29b
8	Me	—	81(1)	122(1)	—	45(1)	^d	25
9	Me	—	63.8(4)	—	—	—	^e	28

^a ΔG and ΔH in kJ mol^{-1} , ΔS in $\text{J mol}^{-1} \text{K}^{-1}$ with estimated standard deviation in parentheses. ^b Estimated from data obtained at 298 K.

^c Extrapolated from data at higher T to 298 K. ^d Liquid or hydrocarbon solution. ^e Mesitylene. ^f Heptane. ^g Xylenes.



Dalton Trans., 2022, 51, 11152–11162 | 11155

due to the volume occupied by the solvent, resulting in reduced translational entropy, as describes by Whitesides and co-workers.¹⁹

The translational entropy correction (tr) combined with the harmonic entropy correction (qh) provides our best estimates of the free energy change, labeled ΔG -qh-tr in Table 3. These combined corrections take us towards the experimentally measured entropies (Table 2). Still, the ΔG -qh-tr values are not in quantitative agreement with experiment though we predict the ease of dissociation correctly ($\text{Me} < \text{Et} \ll \text{i-Bu}$) and in the different solvents (*i.e.* more dissociated in aromatic hydrocarbon due to lower ΔH).

There are several potential reasons for the remaining discrepancy in ΔS between theory and experiment. The experimental values suggest that motion is more restricted in solution than indicated by the approximation in use. The approximation based on free volume indicates an entropy lowering of ΔS -qh-tr – ΔS -qh = $\Delta \Delta S = 43$ – $47 \text{ J mol}^{-1} \text{ K}^{-1}$ for the various solvents at 298 K. We note that another approximation based on the increased density and thus pressure of the liquid state^{16c} leads to $\Delta \Delta S$ values of almost identical magnitude. If we were to further restrict translation using densities typical for organic glasses (*ca.* 1300 kg m^{-3}) we estimate $\Delta \Delta S = 46$ – $50 \text{ J mol}^{-1} \text{ K}^{-1}$ suggesting either approach has limits of this magnitude.

Neither approximation leads to limiting values of ΔS -qh-tr that match experiment. It is possible that rotations are also constrained in the liquid state but the rotational entropy (S -r) of the products ($2 \times 99.7 \text{ J mol}^{-1} \text{ K}^{-1}$ in the case of Me_3Al) might be expected to decrease in proportion to that of the reactant ($119.1 \text{ J mol}^{-1} \text{ K}^{-1}$), where the difference is ΔS -r = $80.3 \text{ J mol}^{-1} \text{ K}^{-1}$ in gas phase at 298 K. A reduction similar to that seen for translations, which we don't think is justified here,³¹ would lead to a further lowering of perhaps no more than $20 \text{ J mol}^{-1} \text{ K}^{-1}$. This would bring us into quantitative agreement with the results of Smith in hydrocarbon media.

Besides being systematically higher, the calculated entropies (for $R = \text{Me}$, ΔS -qh-tr = 141 or $146 \text{ J mol}^{-1} \text{ K}^{-1}$ in aromatic or aliphatic hydrocarbon solution) are insignificantly different in the two different media compared to experiment (*cf.* Table 2, entries 2 and 3). We suspect this also reflects that both products and reactants are specifically solvated, which would have the effect of reducing the entropy further and may account for the significant difference between aromatic *vs.* aliphatic solvents seen experimentally but not theoretically.

We end this section with a discussion of the energetic consequences of specific solvation as studied using the M06-2X and MN15³² functionals, def2-TZVP³³ and def2-TZVPD³⁴ basis sets and CCSD(T) method. The data are summarized in Table 4.

The first entry corresponds to the energy change for dimerization of Me_3Al , which can be thought of as an interaction energy as Me_6Al_2 is energetically the most stable adduct of Me_3Al with itself. The single-point CCSD(T)/def2-TZVPD energies calculated for the MP2/def2-TZVPD optimized geometries provide an instructive reference. At this sophisticated level of theory, the Me_3Al dimerization energy is calculated as -96.5 kJ

Table 4 Interaction energies ΔE (kJ mol^{-1}) of Me_3Al and Me_6Al_2 adducts

Adduct	M06-2X ^a	M06-2X ^b	MN15 ^b	MN15 ^c	CCSD(T) ^d
$\text{Me}_3\text{Al-AlMe}_3$	−92.1	−98.2	−103.7	−104.5	−96.5
$\text{Me}_3\text{Al-C}_7\text{H}_{16}$	−23.8	−23.8	−33.0	−34.2	−25.7
$\text{Me}_3\text{Al-C}_6\text{H}_5\text{CH}_3$	−40.5	−40.8	−48.8	−49.3	−43.4
$\text{Me}_3\text{Al-C}_6\text{H}_3(\text{CH}_3)_3$	−48.2	−48.1	−58.0	−58.6	−51.4
$\text{Me}_3\text{Al-C}_6\text{H}_6$	−36.1	−36.6	−44.0	−44.4	−39.0
$\text{Me}_6\text{Al}_2\text{-C}_6\text{H}_6$	−19.7	−19.5	−25.1	−25.5	−25.4

^a TZVP. ^b def2-TZVP.³³ ^c def2-TZVPD.³⁴ ^d CCSD(T)/def2-TZVPD single-point energy in MP2/def2-TZVPD optimized geometry.

mol^{-1} , which when combined with the quasi-harmonic enthalpy correction calculated at MP2/def2-TZVPD level of theory, gives ΔH -qh = $-84.2 \text{ kJ mol}^{-1}$, *i.e.* in precise match with the experimental enthalpy of 84.2 kJ mol^{-1} for the reverse reaction, quoted from Table 1.

Our method of choice, M06-2X/TZVP underestimates the Me_3Al dimerization energy by *ca.* 4 kJ mol^{-1} (which we already saw in the discussion of Me_3Al dissociation enthalpies, Table 1). While improving the basis set to def2-TZVP might be justified, it has very little effect on the solvent interactions (Table 4, second column), based on which, the effect of specific solvation on dissociation was calculated (Table 3). As for dimerization of Me_3Al , M06-2X is more accurate than MN15, which is consistent with previous evaluations of X_3Al dimerization energies in general.³⁵ However, when it comes to noncovalent interactions, MN15 is better suited to describe those as the Me_6Al_2 -benzene interaction energies are very closely aligned to the CCSD(T) results.

If we consider the specific case of dissociation of Me_6Al_2 in benzene, the dissociation energy is within 4.4 kJ mol^{-1} of the theoretical limiting value, while we underestimate solvation of the Me_3Al product by 2.9 kJ mol^{-1} and of Me_6Al_2 by 5.7 kJ mol^{-1} with respect to the CCSD(T) results. So, overall, our M06-2X/TZVP results are about 7.2 kJ mol^{-1} lower in electronic energy for this reaction than predicted at the CCSD(T) level of theory. This provides some indication of the errors involved when it comes to equilibria involved in larger systems featuring non-covalent interactions, as in the section dealing with metallocenium ion pairs (*vide infra*).

Dissociation of R_6Al_2 *vs.* kinetics of alkyl exchange

The continuing study of the dissociation equilibrium has been motivated by kinetic work focused on the mechanism of exchange of bridging and terminal Al-R groups in these compounds,³⁶ which can be studied by dynamic NMR spectroscopy. There is consensus from this work that the enthalpy of activation decreases in the order $\text{Me} > \text{Et} > \text{higher alkyls}$ and the exchange process is significantly faster in aromatic *vs.* aliphatic media at the same temperature.³⁷ Accepted values for ΔH^\ddagger vary between 63 – 67 kJ mol^{-1} for $R = \text{Me}$ in hydrocarbon media between 263 and 213 K with $\Delta G^\ddagger = 46.0 kJ mol^{-1} at 223 K . An early study featuring the widest temperature range$



provides an estimate of $84 \text{ J mol}^{-1} \text{ K}^{-1}$ for ΔS^\ddagger with $\Delta H^\ddagger = 65.2 \text{ kJ mol}^{-1}$.^{37e}

In earlier work we examined the dissociation of Me_6Al_2 at the M06-2X/TZVP level of theory, and observed a continuous decrease in enthalpy with increasing Al–Al separation, partially offset by a concomitant increase in entropy such that a maximum in $\Delta G^\ddagger = 40.4 \text{ kJ mol}^{-1}$ was observed at 298 K.^{10a} This is in excellent agreement ($\pm 1 \text{ kJ mol}^{-1}$) with experimental values extrapolated from the low temperature NMR data.³⁷ It should be noted that this value is significantly higher than the experimental estimates of ΔG for the dissociation equilibrium at 298 K determined by Černý and coworkers (Table 2, entries 6 and 7) but lower than the value extrapolated by Smith (entry 8) which is inconsistent with their NMR results.

Though there has been a predictable focus on the enthalpy change when discussing the thermodynamics vs. kinetics of the exchange process, and thus its mechanism, it should be noted that the important criterion at any given temperature is that $\Delta G^\ddagger > \Delta G$ and we find this to be the case here.

In comparing *e.g.*, $\text{R} = \text{Me}$ with Et it can be seen in aliphatic media, the principal reason for Et_3Al being more dissociated than Me_3Al at any given temperature is the more favourable entropy increase for the former (Table 3).

Dissociation of $[\text{L}_2\text{ZrMe}_2\text{AlMe}_2]^+$

The solution structure and dynamics of zirconocenium ion-pairs featuring discrete counter-anions has seen intensive experimental and theoretical study.^{2c,d,38} These studies reveal that alkylzirconocenium cations partnered with $[\text{B}(\text{C}_6\text{F}_5)_4]^-$ or related weakly coordinating anions³⁹ typically form CIP in apolar media featuring Zr–F interactions due to the 14 e^- alkylzirconocenium cation. In contrast, 16 e^- cations typically form OSIP in sufficiently dilute solution.³⁸ Also, the CIP can adopt two or more structures featuring different Zr–F interactions,^{38,40} and any equilibrium will thus be weighted by their relative contributions. Finally, specific solvation of the cation in the CIP to form a solvent-separated species has recently been confirmed in toluene solution at least for some complexes of this type.⁴¹ Our particular example involves dis-

sociation of Me_3Al from $[\text{L}_2\text{ZrMe}_2\text{AlMe}_2][\text{B}(\text{C}_6\text{F}_5)_4]^{42}$ in benzene at $T = 313 \text{ K}$ with $\text{L}_2 = \text{Cp}_2$, *rac*-1,2-ethylenebis(η^5 -1-indenyl) (EBI) and $\text{Me}_2\text{C}(\eta^5\text{-C}_5\text{H}_4)_2$ (Me_2CCp_2) (Table 5).⁴³

We should note that the experimental values for K_d and thus ΔG were derived from Dixon plots of the carboalumination rate constants vs. $[\text{Me}_3\text{Al}]$ with the concentration of monomeric Me_3Al being derived from the results of Černý *et al.* at 313 K in mesitylene. Since the two solvents benzene and mesitylene feature different interaction energies with Me_3Al (Table 4), there may be systematic errors involved in this assumption but, not so as to affect the differences in ΔG for the three different ion-pairs (entries 1, 3 and 5).

While the correct order in ΔG -qh-tr is predicted in condensed phase (entries 2, 4 and 6), theory strongly accentuates the differences with ΔG -qh-tr = 11.1 to 31.6 kJ mol^{-1} such that the equilibrium constants would span three orders of magnitude, instead of the experimental results – which do not vary by even one order of magnitude.⁴³ We did investigate using the Boltzmann distribution to weight the theoretical ΔG -qh-tr values according to the stability of isomeric product vs. reactant ion-pairs located by theory but the results did not change significantly (see ESI†).

DFT calculations predict these equilibria involve dissociation of Me_3Al from an OSIP to form a CIP in all three cases (see Fig. 3). For the EBI system where the ligand can adopt forward vs. backward conformations,⁴⁴ we note that the thermodynamically most stable OSIP and CIP adopt the backward conformation. The CIP differ significantly in their geometry about Zr in the three different complexes, reflecting differing interactions with the counter-anion. Only in the case of the Cp_2 system can the anion be considered mono-dentate with a short Zr–F distance of 2.313 Å. There are two other quite long Zr–F contacts of 3.456 and 3.644 Å though both lie within the sum of the crystallographic van der Waals radii of the two elements ($\sim 3.98 \text{ Å}$).⁴⁶ In the case of the Me_2CCp_2 system, the anion can be considered bidentate with two short Zr–o–F distances of 2.349 and 2.739 Å involving different C_6F_5 rings. The longest Zr–F distance involves the central coordination site for an idealized Cp_2ZrL_3 geometry.⁴⁷ The EBI

Table 5 Theory vs. experiment for dissociation of $[\text{L}_2\text{ZrMe}_2\text{AlMe}_2][\text{B}(\text{C}_6\text{F}_5)_4]^a$

Entry	L_2	ΔH	ΔH -qh	ΔG (ΔS)	ΔG -qh (ΔS -qh)	ΔG -qh-tr (ΔS -qh-tr)
$[\text{L}_2\text{ZrMe}_2\text{AlMe}_2][\text{B}(\text{C}_6\text{F}_5)_4] \rightleftharpoons \text{Me}_3\text{Al} + [\text{L}_2\text{ZrMe}][\text{B}(\text{C}_6\text{F}_5)_4]$ (benzene solution, 313 K)						
1	Cp_2	—	—	20.0(3)	20.0(3)	20.0(3)
2	Cp_2	75.9	76.9	10.0 (210)	9.7 (215)	24.2 (168)
3	EBI	—	—	23.8(4)	23.8(4)	23.8(4)
4	EBI	81.0	82.3	15.8 (208)	17.0 (209)	31.6 (162)
5	Me_2CCp_2	—	—	18.7(3)	18.7(3)	18.7(3)
6	Me_2CCp_2	59.8	61.4	0.1 (191)	−3.5 (207)	11.1 (161)
$[\text{L}_2\text{ZrMe}_2\text{AlMe}_2][\text{B}(\text{C}_6\text{F}_5)_4] \cdot \text{C}_6\text{H}_6 + \text{C}_6\text{H}_6 \rightleftharpoons \text{Me}_3\text{Al} \cdot \text{C}_6\text{H}_6 + [\text{L}_2\text{ZrMe}(\text{C}_6\text{H}_6)][\text{B}(\text{C}_6\text{F}_5)_4]$ (benzene solution, 313 K)						
7	Cp_2	64.0	67.5	10.2 (172)	3.7 (204)	18.2 (157)
8 ^b	Cp_2	64.2	68.2	12.4 (166)	4.3 (204)	18.9 (157)
9	EBI	47.8	48.3	30.0 (57.0)	27.3 (67.1)	27.3 (67.1)
10	Me_2CCp_2	36.3	36.2	16.8 (62.2)	14.1 (70.5)	14.1 (70.5)

^a ΔG and ΔH in kJ mol^{-1} , ΔS in $\text{J mol}^{-1} \text{ K}^{-1}$ with estimated standard deviation in parentheses where applicable. ^b Includes specific solvation of the reactant ion-pair by two benzene molecules.



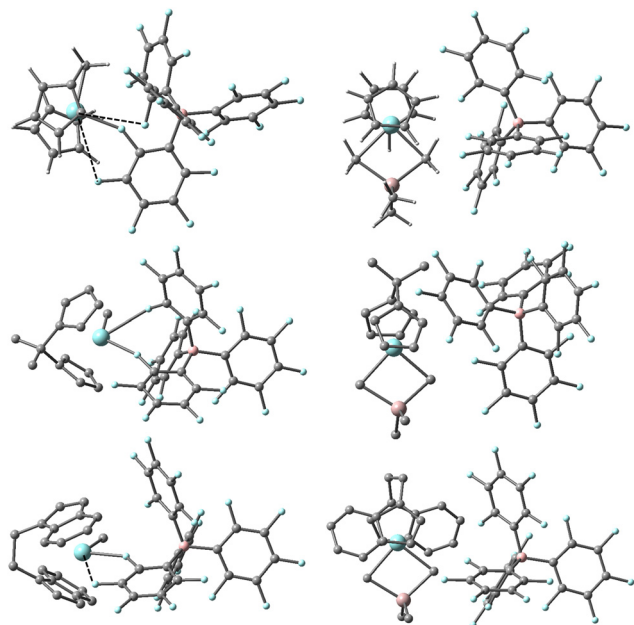
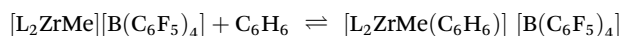


Fig. 3 Most stable structures of $[\text{L}_2\text{ZrMe}][\text{B}(\text{C}_6\text{F}_5)_4]$ ($\text{L}_2 = \text{Cp}_2$,⁴⁵ Me_2CCp_2 and EBI, left) and $[\text{L}_2\text{ZrMe}_2\text{AlMe}_2][\text{B}(\text{C}_6\text{F}_5)_4]$ (right) based on Gibbs energy ($\Delta G\text{-qh-tr}$) at the M062-X/TZVP level of theory. Zr and F in blue, Al and B in pink, C in grey, H omitted from lower two structures for clarity. Long Zr–F contacts are shown as dashed lines.

system is intermediate between these extremes with one short ($\text{Zr-}o\text{-F} = 2.335 \text{ \AA}$) and one longer ($\text{Zr-}m\text{-F} = 3.117 \text{ \AA}$) contact involving the same C_6F_5 ring. We should note that similar structures have been detected in simulations involving $[\text{Me}_2\text{SiCp}_2\text{ZrMe}][\text{B}(\text{C}_6\text{F}_5)_4]$ at a lower level of theory.⁴⁰ We suspect these different interactions between anion and cation lead to the larger spread in free energy differences for the different ligands, while the experimental results suggest the involvement of species in which the effect of the anion has been mitigated to some extent.

We thus considered specific solvation of reactant *vs.* product ion-pairs by benzene. We found that both the Zr cation and the anion were susceptible to specific solvation, though inclusion of two benzene moieties led to results that were not significantly different compared to just one (Table 5, entry 7 *vs.* 8). In some CIP structures the coordinated benzene was also involved in arene-perfluoroarene interactions with the anion⁴⁸ (see ESI,[†] *e.g.* $[\text{Cp}_2\text{ZrMe}][\text{B}(\text{C}_6\text{F}_5)_4]$ -benzene isomer 2). Inclusion of specific solvation has the desired effect as we move closer to experiment in all three cases, where the differences now result in K_d values that differ by less than 160 at 313 K. We should temper this positive result by stating that binding of benzene to the thermodynamically most stable CIP (and also OSIP) is endergonic with $\Delta G\text{-qh-tr} = 6.7$ to 16.1 kJ mol^{-1} for the equilibrium:



However, since we underestimate the $\text{Me}_2\text{Al}_2\text{-C}_6\text{H}_6$ interaction energy at the M06-2X/TZVP level of theory by 5.7 kJ mol^{-1} (Table 4), it is probable that we underestimate enthalpy

changes at least by the same amount for equilibria of this type. We hesitate to apply any quantitative correction and conclude that specific solvation is undoubtedly important.

Dissociation of $[(\text{L}_2\text{ZrMe})_2\text{Me}]^+$

Our third and final test equilibrium is dissociation of $\text{Cp}''_2\text{ZrMe}_2$ from $[(\text{Cp}''_2\text{ZrMe})_2\mu\text{-Me}][\text{MePBB}]$ ($\text{Cp}'' = 1,2\text{-Me}_2\text{C}_5\text{H}_3$, PBB = tris-(perfluorobiphenyl)borane) in toluene.⁴⁹ This dinuclear ion-pair was fully characterized in solution and the solid state. The dinuclear cation features an *s-gauche* geometry¹⁵ with a dihedral angle $\text{Me-Zr}\cdots\text{Zr-Me}$ angle $\varphi = 108.5^\circ$ and a near linear geometry for the $\mu\text{-Me}$ bridge ($\angle\text{ZrMeZr} = 170.9^\circ$). However, we find in the presence of the counter-anion in gas phase and toluene continuum that a *syn* isomer with $\angle\text{ZrMeZr} = 171.0^\circ$ and $\varphi = 37.7^\circ$ (Fig. 4) is most stable electronically, compared to two *anti* stereoisomers with $\Delta E = 7.4$ and 9.0 kJ mol^{-1} . The higher energy of these corresponded to the X-ray structure.

In comparing the two structures, it is obvious that the theoretical structure has a much closer contact of the anion with the cation, as would be expected for an isolated ion-pair in gas or condensed phase in a low dielectric medium.

In earlier work, several limiting conformers were located for dinuclear cations of this type with the stability of the *syn* isomers ($\varphi < 90^\circ$) *vs.* the *anti* conformers ($\varphi > 90^\circ$) being dependent on ligand structure in gas phase.^{15,50} Thus, the X-ray structure more closely resembles the situation in gas or condensed phase of an isolated cation, while our DFT results suggest that close contact of anion and cation induces a conformational change in the latter.

In discussing the dissociation equilibrium we considered three *anti* and *syn* $[(\text{Cp}''_2\text{ZrMe})_2\mu\text{-Me}][\text{MePBB}]$ stereoisomers located by theory. The results are summarized in Table 6.

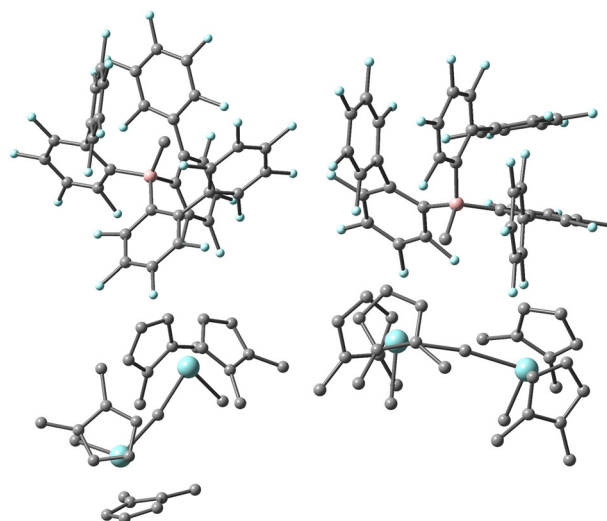


Fig. 4 X-ray structure of $[(\text{Cp}''_2\text{ZrMe})_2\mu\text{-Me}][\text{MePBB}]$ ($\text{Cp}'' = 1,2\text{-Me}_2\text{C}_5\text{H}_3$, PBB = tris-(perfluorobiphenyl)borane) (left) and thermodynamically most stable structure (right) located by DFT. Zr and F in blue, B in pink, C in grey, H omitted for clarity.



Table 6 Theory vs. experiment for dissociation of $[(\text{Cp}''_2\text{ZrMe})_2\mu\text{-Me}][\text{MePBB}]^a$

syn or anti- $[(\text{Cp}''_2\text{ZrMe})_2\mu\text{-Me}][\text{MePBB}] \rightleftharpoons \text{Cp}''_2\text{ZrMe}_2 + [\text{Cp}''_2\text{ZrMe}][\text{Me(PBB)}]$ ($\text{Cp}'' = \eta^5\text{-1,2-Me}_2\text{C}_5\text{H}_3$, toluene solution, 298 K)											
Entry	Isomer	ΔH	$\Delta H\text{-qh}$	ΔS	$\Delta S\text{-qh}$	$\Delta S\text{-tr}$	$\Delta S\text{-qh-tr}$	ΔG	$\Delta G\text{-qh}$	$\Delta G\text{-tr}$	$\Delta G\text{-qh-tr}$
1	<i>syn</i>	53.4	59.3	173	236	126	190	1.3	−11.1	15.1	2.7
2	<i>anti</i>	46.3	50.7	198	245	151	198	−13.2	−22.3	0.6	−8.4
3	<i>anti</i> ^b	42.9	48.5	154	247	107	200	2.9	−25.0	10.9	−11.2
Experiment		42.9(8)	42.9(8)	110(17)	110(17)	110(17)	110(17)	10.1(2)	10.1(2)	10.1(2)	10.1(2)

^a ΔG and ΔH in kJ mol^{-1} , ΔS in $\text{J mol}^{-1} \text{K}^{-1}$ with estimated standard deviation in parentheses where applicable. ^b Geometry corresponds to the X-ray structure.⁴⁹

When it comes to ΔH the experimental result is significantly lower than theory would indicate for the *syn* stereoisomer, while better agreement is seen for either *anti* stereoisomer, especially that corresponding to the X-ray structure. We thus hypothesize that rotamers of both types are present in toluene solution, and to the extent that *anti* isomers contribute to the dissociation equilibrium, one can expect the ΔH to decrease. We do note that correction for low energy vibrations in all cases moves $\Delta H\text{-qh}$ away from experiment.

Similarly, $\Delta S\text{-qh}$ also moves in the wrong direction, away from both experiment when lower energy vibrations are approximated for in this case. The poor agreement between calculated and experimental entropy may be related to the somewhat arbitrary cut-off frequency of 100 cm^{-1} . For example, using 50 and 150 cm^{-1} cut-offs for the *syn* stereoisomer, $\Delta S\text{-qh} = 180$ and $218 \text{ J mol}^{-1} \text{K}^{-1}$, respectively. Based on these numbers, it is clear how sensitive the vibrational entropy really is for systems of this size and complexity. In fact, if we just correct for the translational entropy, we obtain estimates of $\Delta S\text{-tr}$ that are in reasonable agreement with experiment, while inclusion of both translation and vibrational entropy corrections moves us further away.

We did locate six low energy isomers of the product ion-pair $[\text{Cp}''_2\text{ZrMe}][\text{Me(PBB)}]$ within 10 kJ mol^{-1} of the minimum and also the neutral $\text{Cp}''_2\text{ZrMe}_2$ by-product can adopt two low energy conformations in toluene continuum, both involving rotations about the Cp' rings. In this case, use of the $\Delta G\text{-tr}$ values, which seem especially close to experiment, weighted by the Boltzmann distribution leads to an averaged value $\Delta G\text{-tr} = 15.3 \text{ kJ mol}^{-1}$. However, it was prohibitive to locate all low energy isomers of the dinuclear ion-pair, due to the presence of many low energy conformations available to the $1,2\text{-Me}_2\text{C}_5\text{H}_3$ rings (with each a five-fold rotor there are $5^4 = 625$ unique conformers in the presence of the anion). Similarly, treatment of specific solvation by toluene is much more complicated in this case given these distinguishing features. Hence, a more exact treatment is not possible.

Conclusions

Taking this all together, we have shown that experimental reaction enthalpies are well produced by the M06-2X/TZVP method, both in gas-phase and in solution, provided in the latter case that specific solvent interactions are taken into con-

sideration. However, entropy and hence free energy poses a great challenge for theory, and even more so in solution.

To understand the difficulty in accurate calculation of entropy, the vibrational, translational, and rotational contributions must be studied separately. Concerning vibrations, low-energy ($<100 \text{ cm}^{-1}$) normal modes make a significant contribution to entropy at room temperature, but since they cannot be calculated to precision using a harmonic oscillator approximation, the resulting entropies vary widely even within different conformers without genuine physical significance. A partial remedy for this general problem is to get rid of the low-energy normal modes using a quasi-harmonic entropy correction, *e.g.*, by raising each of them to the same energy (*e.g.*, 100 cm^{-1}). This approach improves accuracy for small systems such as those involved in R_6Al_2 dissociation equilibrium (Table 1). However, as demonstrated for dissociation of $[(\text{Cp}''_2\text{ZrMe})_2\mu\text{-Me}][\text{MePBB}]$ (Table 6), it is troublesome for complicated systems, such as reactions involving ion pairs, because the number of low-energy vibrations is so large (for the reactant there are >30 normal modes below the arbitrary threshold of 100 cm^{-1}) that the quasi-harmonic correction leads to significant artificial lowering of the total entropy, and as consequence, to significant increase in the reaction entropy in this specific case.

Entropy is reduced on moving from gas-phase to solution, which mostly originates from suppression of translations. Since this is neglected by the polarizable continuum model calculations, it needs to be considered separately. We evaluated two previously proposed approaches, which produced consistent entropy reductions, though not quite large enough to quantitatively match with the experimental observations.

Finally, we note that although the primary motivation of this work was to set up the path for detailed computational investigation of metallocene-MAO catalyst activation, the expressed concerns regarding entropy computations should be considered universal. The arbitrariness of vibrational entropy and its consequences on free energy of large systems need to be recognized, and methodologies for reliable calculation of solution entropy require further consideration.

Experimental section

DFT calculations

Geometry optimizations and electronic energy calculations were employed by the M06-2X density functional,⁷ in conjunc-



tion with the TZVP basis set.⁸ Interaction energies summarized in Table 4 employed in addition the MN15 density functional³² in combination with a def2-TZVP³³ or def2-TZVPD³⁴ basis set, and frozen-core CCSD(T)/def2-TZVPD single point calculations carried out at MP2/def2-TZVPD optimized geometries. Relativistic effective core potential of 28 electrons was used to describe the core electrons of Zr.⁵⁵ Polarizable continuum model calculations were employed by the integral equation formalism variant (IEFPCM).³⁰ We also tested the SMD variation of IEFPCM,⁵¹ with similar results, but decided to abandon it due to significant convergence issues. Stationary points were confirmed as minima by harmonic vibrational frequency calculations. All calculations were carried out using Gaussian 16.⁵²

Quasi-harmonic corrections to the entropy¹⁴ and enthalpy²³ were employed using cut-off frequency of 100 cm⁻¹ and corrections to reduced translational entropy in solution were calculated by the method described by Whitesides *et al.*¹⁹ All the corrections were employed using the Goodvibes script,⁵³ modified to include molarities and molecular volumes of the solvents, which were required for calculation of free accessible space.⁵⁴

Author contributions

M. L. carried out the quantum chemical calculations. M. L. and S. C. jointly aligned theory with experiments and co-wrote the manuscript.

Conflicts of interest

There are no conflicts to declare.

Acknowledgements

M. L. acknowledges the Academy of Finland Flagship Programme, Photonics Research and Innovation (PREIN), decision 320166. Computations were made possible by use of the Finnish Grid and Cloud Infrastructure resources (urn:nbn:fi:research-infras-2016072533).

Notes and references

- Recent aluminosilicate literature: (a) A. F. R. Kilpatrick, H. S. Geddes, Z. R. Turner, J.-C. Buffet, A. L. Goodwin and D. O'Hare, *Catal. Sci. Technol.*, 2021, **11**, 5472–5483; (b) R. Tanaka, M. Nishizono, Y. Nakayama and T. Shiono, *Polym. J.*, 2021, **53**, 1187–1193; (c) T. V. Tyumkina, D. N. Islamov, P. V. Kovyazin and L. V. Parfenova, *Mol. Catal.*, 2021, **512**, 111768; (d) F. Zaccaria, C. Zuccaccia, R. Cipullo, P. H. M. Budzelaar, A. Macchioni, V. Busico and C. Ehm, *Eur. J. Inorg. Chem.*, 2020, 1088–1095; (e) F. Zaccaria, P. H. M. Budzelaar, R. Cipullo, C. Zuccaccia, A. Macchioni, V. Busico and C. Ehm, *Inorg. Chem.*, 2020, **59**, 5751–5759; (f) J. V. Lamb, J.-C. Buffet, Z. R. Turner and D. O'Hare, *Macromolecules*, 2020, **53**, 929–935; (g) A. F. R. Kilpatrick, N. H. Rees, Z. R. Turner, J. C. Buffet and D. O'Hare, Physicochemical surface-structure studies of highly active zirconocene polymerisation catalysts on solid polymethylaluminumoxane activating supports, *Mater. Chem. Front.*, 2020, **4**, 3226–3233; (h) V. E. Teixeira and P. R. Livotto, *J. Mol. Graphics Modell.*, 2020, **99**, 107626; (i) M. E. Z. Velthoen, J. M. Boereboom, R. E. Bulo and B. M. Weckhuysen, *Catal. Today*, 2019, **334**, 223–230; (j) M. E. Z. Velthoen, A. Muñoz-Murillo, A. Bouhmadi, M. Cecius, S. Diefenbach and B. M. Weckhuysen, *Macromolecules*, 2018, **51**, 343–355; (k) Z. Falls, E. Zurek and J. Autschbach, *Phys. Chem. Chem. Phys.*, 2016, **18**, 24106–24118.
- Reviews: (a) H. S. Zijlstra and S. Harder, *Eur. J. Inorg. Chem.*, 2015, 19–43; (b) W. Kaminsky, *Macromolecules*, 2012, **45**, 3289–3297; (c) M. Bochmann, *Organometallics*, 2010, **29**, 4711–4740; (d) E. Y.-X. Chen and T. J. Marks, *Chem. Rev.*, 2000, **100**, 1391–1434.
- See e.g. (a) E. Zurek and T. Ziegler, *Prog. Polym. Sci.*, 2004, **29**, 107–148; (b) Z. Boudene, T. De Bruin, H. Toulhoat and P. Raybaud, *Organometallics*, 2012, **31**, 8312–8322; (c) Z. Falls, N. Tymińska and E. Zurek, *Macromolecules*, 2014, **47**, 8556–8569.
- (a) L. Negureanu, R. W. Hall, L. G. Butler and L. A. Simeral, *J. Am. Chem. Soc.*, 2006, **128**, 16816–16826; (b) M. Linnolahti, J. R. Severn and T. A. Pakkanen, *Angew. Chem., Int. Ed.*, 2008, **47**, 9279–9283; (c) R. Glaser and X. Sun, *J. Am. Chem. Soc.*, 2011, **133**, 13323–13336; (d) M. Linnolahti, A. Laine and T. A. Pakkanen, *Chem. – Eur. J.*, 2013, **19**, 7133–7142; (e) J. T. Hirvi, M. Bochmann, J. R. Severn and M. Linnolahti, *ChemPhysChem*, 2014, **15**, 2732–2742.
- S. Collins, A. Joshi and M. Linnolahti, *Chem. – Eur. J.*, 2021, **27**, 15460–15471.
- M. Linnolahti and S. Collins, *ChemPhysChem*, 2017, **18**, 3369–3374.
- Y. Zhao and D. G. Truhlar, *Theor. Chem. Acc.*, 2008, **120**, 215–241.
- A. Schäfer, C. Huber and R. Ahlrichs, *J. Chem. Phys.*, 1994, **100**, 5829–5835.
- C. Ehm, G. Antinucci, P. H. M. Budzelaar and V. Busico, *J. Organomet. Chem.*, 2014, **772–773**, 161–171.
- (a) H. S. Zijlstra, A. Joshi, M. Linnolahti, S. Collins and J. S. McIndoe, *Eur. J. Inorg. Chem.*, 2019, 2346–2355; (b) H. S. Zijlstra, M. Linnolahti, S. Collins and J. S. McIndoe, *Organometallics*, 2017, **36**, 1803–1809; (c) S. Collins, M. Linnolahti, M. G. Zamora, H. S. Zijlstra, M. T. R. Hernández and O. Perez-Camacho, *Macromolecules*, 2017, **50**, 8871–8884; (d) T. K. Trefz, M. A. Henderson, M. Linnolahti, S. Collins and J. S. McIndoe, *Chem. – Eur. J.*, 2015, **21**, 2980–2991; (e) T. K. Trefz, M. A. Henderson, M. Wang, S. Collins and J. S. McIndoe, *Organometallics*, 2013, **32**, 3149–3152.
- (a) D. E. Babushkin, N. V. Semikolenova, V. N. Panchenko, A. P. Sobolev, V. A. Zakharov and E. P. Talsi, *Macromol.*



- Chem. Phys.*, 1997, **198**, 3845–3854; (b) I. Tritto, C. Méalares, M. C. Sacchi and P. Locatelli, *Macromol. Chem. Phys.*, 1997, **198**, 3963–3977.
- 12 H. S. Zijlstra, A. Joshi, M. Linnolahti, S. Collins and J. S. McIndoe, *Dalton Trans.*, 2018, **47**, 17291–17298.
- 13 (a) A. Joshi, S. Collins, M. Linnolahti, H. S. Zijlstra, E. Liles and J. S. McIndoe, *Chem. – Eur. J.*, 2021, **27**, 8753–8763; (b) S. Collins, G. Hasan, A. Joshi, J. S. McIndoe and M. Linnolahti, *ChemPhysChem*, 2021, **22**, 1326–1335.
- 14 R. F. Ribeiro, A. V. Marenich, C. J. Cramer and D. G. Truhlar, *J. Phys. Chem. B*, 2011, **115**, 14556–14562.
- 15 S. Collins and M. Linnolahti, *ChemCatChem*, 2022, **14**, e202101918 and references therein.
- 16 See e.g. (a) J. N. Harvey, F. Himo, F. Maseras and L. Perrin, *ACS Catal.*, 2019, **9**, 6803–6813; (b) M. Besora, P. Vidossich, A. Lledós, G. Ujaque and F. Maseras, *J. Phys. Chem. A*, 2018, **122**, 1392–1399; (c) L. Falivene, V. Barone and G. Talarico, *Mol. Catal.*, 2018, **452**, 138–144.
- 17 (a) S. Tobisch and T. Ziegler, *J. Am. Chem. Soc.*, 2004, **126**, 9059–9071; (b) F. Zaccaria, C. Ehm, P. H. M. Budzelaar and V. Busico, *ACS Catal.*, 2017, **7**, 1512–1519; (c) F. Zaccaria, R. Cipullo, P. H. M. Budzelaar, V. Busico and C. Ehm, *J. Polym. Sci., Part A: Polym. Chem.*, 2017, **55**, 2807–2814.
- 18 J. Tomasi, B. Mennucci and R. Cammi, *Chem. Rev.*, 2005, **105**, 2999–3093.
- 19 M. Mammen, E. I. Shakhnovich, J. M. Deutch and G. M. Whitesides, *J. Org. Chem.*, 1998, **63**, 3821–3830.
- 20 See J. J. Eisch, in *Comprehensive Organometallic Chemistry*, ed. G. Wilkinson, F. G. A. Stone and E. W. Abel, Pergamon Press, London, 1982, vol. 1, ch. 6, pp. 555–682.
- 21 (a) C. H. Henrickson and D. P. Eyman, *Inorg. Chem.*, 1967, **6**, 1461–1465; (b) A. W. Laubengayer and W. F. Gilliam, *J. Am. Chem. Soc.*, 1941, **63**, 477–479.
- 22 L. A. Watson and O. Eisenstein, *J. Chem. Educ.*, 2002, **79**, 1269–1277.
- 23 Y.-P. Li, J. Gomes, S. M. Sharada, A. T. Bell and M. Head-Gordon, *J. Phys. Chem. C*, 2015, **119**, 1840–1850.
- 24 W. F. Gilliam, PhD thesis, Cornell University, 1939.
- 25 M. B. Smith, *J. Organomet. Chem.*, 1972, **46**, 31–49.
- 26 In terms of G -qh, we calculated the C_{2h} -symmetric minimum 4.5 kJ mol^{−1} higher, and two C_1 -symmetric minima 4.6 and 6.6 kJ mol^{−1} higher than the C_s -symmetric minimum, see: L. Verrieux, J. Thuilliez, F. Jean-Baptiste-dit-Dominique, C. Boisson, M.-N. Poradowski and L. Perrin, *ACS Catal.*, 2020, **10**, 12359–12369.
- 27 M. B. Smith, *J. Organomet. Chem.*, 1970, **22**, 273–281.
- 28 M. B. Smith, *J. Organomet. Chem.*, 1972, **46**, 211–217.
- 29 (a) Z. Černý, S. Heřmánek, J. Fusek, O. Kříž and B. Čásenský, *J. Organomet. Chem.*, 1988, **345**, 1–9; (b) Z. Černý, J. Fusek, O. Kříž, S. Heřmánek, M. Šolc and B. Čásenský, *J. Organomet. Chem.*, 1990, **386**, 157–165.
- 30 G. Scalmani and M. J. Frisch, *J. Chem. Phys.*, 2010, **132**, 114110.
- 31 M. S. Searle and D. H. Williams, *J. Am. Chem. Soc.*, 1992, **114**, 10690–10697.
- 32 H. S. Yu, X. He, S. L. Li and D. G. Truhlar, *Chem. Sci.*, 2016, **7**, 5032–5051.
- 33 F. Weigend and R. Ahlrichs, *Phys. Chem. Chem. Phys.*, 2005, **7**, 3297–3305.
- 34 D. Rappoport and F. Furche, *J. Chem. Phys.*, 2010, **133**, 134105.
- 35 (a) Y. Wang, P. Verma, X. Jin, D. G. Truhlar and X. He, *Proc. Natl. Acad. Sci. U. S. A.*, 2018, **115**, 10257–10262; (b) L. Goerigk, A. Hansen, C. Bauer, S. Ehrlich, A. Najibi and S. Grimme, *Phys. Chem. Chem. Phys.*, 2017, **19**, 32184–32215.
- 36 D. S. Matteson, *Organometallic Reaction Mechanisms of the Non-transition Elements*, Academic Press, New York, 1974, ch. 2, pp. 34–58.
- 37 (a) O. Yamamoto, R. Hayamizu and M. Yanagisawa, *J. Organomet. Chem.*, 1974, **73**, 17–25; (b) E. A. Jeffery and T. Mole, *Aust. J. Chem.*, 1973, **26**, 739–748; (c) T. L. Brown and L. L. Murrell, *J. Am. Chem. Soc.*, 1972, **94**, 378–384; (d) D. S. Matteson, *Inorg. Chem.*, 1971, **10**, 1555; (e) C. Ramey, J. F. O'Brien, I. Hasegawa and A. E. Borchert, *J. Phys. Chem.*, 1965, **69**, 3418–3423.
- 38 Review: F. Zaccaria, L. Sian, C. Zuccaccia and A. Macchioni, in *Advances in Organometallic Chemistry*, ed. P. J. Perez, Academic Press, 2020, vol. 73, ch. 1, pp. 1–78.
- 39 For recent examples see e.g. (a) S. O. Gunther, Q. Lai, T. Senecal, R. Huacuja, S. Bremer, D. M. Pearson, J. C. DeMott, N. Bhuvanesh, O. V. Ozerov and J. Klosin, *ACS Catal.*, 2021, **11**, 3335–3342; (b) T. Nakashima, Y. Nakayama, T. Shiono and R. Tanaka, *ACS Catal.*, 2021, **11**, 865–870.
- 40 A. Correa and L. Cavallo, *J. Am. Chem. Soc.*, 2006, **128**, 10952–10959.
- 41 L. Sian, A. Dall'Anese, A. Macchioni, L. Tensi, V. Busico, R. Cipullo, G. P. Goryunov, D. Uborsky, A. Z. Voskoboynikov, C. Ehm, L. Rocchigiani and C. Zuccaccia, *Organometallics*, 2022, **41**, 547–560 and references therein.
- 42 M. Bochmann and S. J. Lancaster, *Angew. Chem., Int. Ed. Engl.*, 1994, **33**, 1634–1637.
- 43 J. M. Camara, R. A. Petros and J. R. Norton, *J. Am. Chem. Soc.*, 2011, **133**, 5263–5273.
- 44 Theory: (a) M. Linnolahti, T. A. Pakkanen, R. Leino, H. J. G. Luttikhedde, C.-E. Wilén and J. H. Näsman, *Eur. J. Inorg. Chem.*, 2001, 2033–2040 and references therein; Experiment: (b) F. Piemontesi, I. Camurati, L. Resconi, D. Balboni, A. Sironi, M. Moret, R. Zeigler and N. Piccolrovazzi, *Organometallics*, 1995, **14**, 1256–1266.
- 45 A. Laine, B. B. Coussens, J. T. Hirvi, A. Berthoud, N. Friederichs, J. R. Severn and M. Linnolahti, *Organometallics*, 2015, **34**, 2415–2421.
- 46 S. Alvarez, *Dalton Trans.*, 2013, **42**, 8617–8636.
- 47 J. W. Lauher and R. Hoffmann, *J. Am. Chem. Soc.*, 1976, **98**, 1729–1742.
- 48 C. E. Smith, P. S. Smith, R. Ll. Thomas, E. G. Robins, J. C. Collings, C. Dai, A. J. Scott, S. Borwick, A. S. Batsanov,



- S. W. Watt, S. J. Clark, C. Viney, J. A. K. Howard, W. Clegg and T. B. Marder, *J. Mater. Chem.*, 2004, **14**, 413–420.
- 49 (a) Y.-X. Chen, M. V. Metz, C. L. Stern and T. J. Marks, *J. Am. Chem. Soc.*, 1998, **120**, 6287–6305. For earlier work see ref. 42 and. S. Beck, M.-H. Prosenc, H.-H. Brintzinger, R. Goretzki, N. Herfert and G. Fink, *J. Mol. Catal. A: Chem.*, 1996, **111**, 67–79.
- 50 W. Meelua, N. Keawkla, J. Oláh and J. Jitonnorn, *J. Organomet. Chem.*, 2020, **905**, 121024.
- 51 A. V. Marenich, C. J. Cramer and D. G. Truhlar, *J. Phys. Chem. B*, 2009, **113**, 6378–6396.
- 52 M. J. Frisch, G. W. Trucks, H. B. Schlegel, G. E. Scuseria, M. A. Robb, J. R. Cheeseman, G. Scalmani, V. Barone, G. A. Petersson, H. Nakatsuji, X. Li, M. Caricato, A. V. Marenich, J. Bloino, B. G. Janesko, R. Gomperts, B. Mennucci, H. P. Hratchian, J. V. Ortiz, A. F. Izmaylov, J. L. Sonnenberg, D. Williams-Young, F. Ding, F. Lipparini, F. Egidi, J. Goings, B. Peng, A. Petrone, T. Henderson, D. Ranasinghe, V. G. Zakrzewski, J. Gao, N. Rega, G. Zheng, W. Liang, M. Hada, M. Ehara, K. Toyota, R. Fukuda, J. Hasegawa, M. Ishida, T. Nakajima, Y. Honda, O. Kitao, H. Nakai, T. Vreven, K. Throssell, J. A. Montgomery Jr., J. E. Peralta, F. Ogliaro, M. J. Bearpark, J. J. Heyd, E. N. Brothers, K. N. Kudin, V. N. Staroverov, T. A. Keith, R. Kobayashi, J. Normand, K. Raghavachari, A. P. Rendell, J. C. Burant, S. S. Iyengar, J. Tomasi, M. Cossi, J. M. Millam, M. Klene, C. Adamo, R. Cammi, J. W. Ochterski, R. L. Martin, K. Morokuma, O. Farkas, J. B. Foresman and D. J. Fox, *Gaussian 16, Revision A.03*, Gaussian, Inc., Wallingford CT, 2016.
- 53 G. Luchini, J. V. Alegre-Requena, Y. Guan, I. Funes-Ardoiz and R. S. Paton, *GoodVibes, Version 3.0.1*, 2019, DOI: [10.5281/zenodo.595246](https://doi.org/10.5281/zenodo.595246).
- 54 The following molarities (mol dm⁻³)/molecular volumes (Å³) were used: toluene: 9.4/138.4; benzene: 11.2/116.4; mesitylene: 7.19/181.9; heptane: 6.82/184.1. Volumes were calculated by Gaussian 16 using tight option and an average of ten volume calculations was used.
- 55 D. Andrae, U. Haeussermann, M. Dolg, H. Stoll and H. Preuss, *Theor. Chim. Acta*, 1990, **77**, 123–141.

